

1 **Degradation induced by recycled Construction and Demolition Wastes**
2 **on the short-term tensile behaviour of two geosynthetics**

3

4 Castorina Silva Vieira^{1,#} and Paulo M. Pereira¹

5

6 ¹*University of Porto – Faculty of Engineering*

7 *Department of Civil Engineering*

8 *R. Dr. Roberto Frias, 4200-465 Porto, Portugal*

9

10

11 **ABSTRACT**

12 Geosynthetics have been used as a reinforcement material in roadways and railways
13 construction. Notwithstanding, one of the main questions of using is their durability.

14 The damage caused by the mechanical actions during installation and the chemical and
15 biological degradation are important issues to consider in the physical, mechanical and
16 hydraulic behaviour of geosynthetics. The change in their properties induced by these
17 degradation processes can compromise the performance of these materials. In order to
18 study the chemical and environmental degradation induced by a recycled Construction

Corresponding author. Tel.: +351 225081586; Fax: +351 225081446

E-mail address: cvieira@fe.up.pt

19 and Demolition Waste (C&DW) on the short-term tensile behaviour of two
20 geosynthetics (a uniaxial HDPE geogrid and a nonwoven PP geotextile reinforced with
21 PET yarns) used commonly as reinforcement material, a damage trial embankment (2m
22 x 3m in plant) was constructed. This paper presents and discusses the effects produced
23 by the recycled C&DW on geosynthetic samples exhumed after 6 months of the
24 embankment construction. The constituents and the leaching behaviour of the recycled
25 C&DW are presented. Wide width tensile tests were performed on exhumed and intact
26 (as-received) geosynthetics and their tensile behaviour is compared. Scanning electron
27 microscope (SEM) images of intact and exhumed specimens are also presented. As
28 expected the degradation induced by the recycled C&DW after 6 months of exposure is
29 not very expressive. On the HDPE geogrid the recycled C&DW induced a small
30 decrease on the tensile strength and the reduction of the tensile stiffness modulus. The
31 geocomposite experienced some reduction on the tensile strength (16% on average) but
32 the effects on tensile stiffness and shape of the load-strain curves were not significant.

33

34

35 **KEYWORDS:** Construction and Demolitions materials; Recycled aggregates;

36 Geosynthetics; Environmental degradation; Damage trial embankment

37

38

39

40

41 NOTATION

- 42 J - geosynthetic axial stiffness (kN/m)
- 43 $J_{2\%}$ - secant stiffness modulus at strain of 2% (kN/m)
- 44 $J_{T_{max}}$ - secant stiffness modulus at $\epsilon_{T_{max}}$ (kN/m)
- 45 RF_{ID} - installation damage reduction factor (dimensionless)
- 46 RF_{CR} - creep reduction factor (dimensionless)
- 47 RF_D - durability reduction factor (dimensionless)
- 48 RF_W - reduction factor for weathering (dimensionless)
- 49 RF_{CH} - reduction factor for chemical/environmental effects (dimensionless)
- 50 R_T - retained tensile strength (dimensionless)
- 51 R_ϵ - retained peak strain (dimensionless)
- 52 $R_{J_{2\%}}$ - retained secant modulus at 2% of strain (dimensionless)
- 53 T - load per unit width (kN/m)
- 54 T_{al} - available long-term tensile strength (kN/m)
- 55 T_{max} - geosynthetic tensile strength or maximum tensile force (kN/m)
- 56 T_{nom} - nominal tensile strength of geosynthetic (value declared by the producer)
- 57 (kN/m)
- 58 T_{ult} - ultimate tensile strength (kN/m)
- 59 ϵ - geosynthetic strain (dimensionless)
- 60 $\epsilon_{T_{max}}$ - geosynthetic strain for T_{max} (dimensionless)

61 1. INTRODUCTION

62 Granular materials are commonly used in civil engineering applications, such as
63 embankments, retaining walls, road bases and railway ballast. In addition, over the last
64 years the environmental sustainability has been demanding a progressive increase in the
65 waste recycling in general and in the waste valorisation in construction industry, in
66 particular. Some studies and applications of recycled Construction and Demolition
67 materials have been performed in recent years, mainly related to the production of
68 aggregates for use in concrete and in base and sub-base layers of transportation
69 infrastructures (Jiménez et al. 2012; Arulrajah et al. 2013a; Rahman et al. 2013;
70 Rahman et al. 2015).

71 Construction and Demolition materials have been found to be viable alternative
72 materials in applications such as pavement sub-bases and other road construction
73 applications (Arulrajah et al. 2013a). However, the properties of these alternative
74 materials is not fully understood compared to natural quarried materials, and, hence,
75 their usage continues to face many barriers (Arulrajah et al. 2013b).

76 Geosynthetics, particularly geogrids and high strength geotextiles, are used as a
77 reinforcement material in various geotechnical engineering applications such as roads
78 and railway embankments. Consequently, the assessment of their behaviour during and
79 after exposition to recycled C&DW is an important research issue to overcome the
80 barriers on the usage of recycled aggregates.

81 The durability is one of the main questions on the use of geosynthetics in ground
82 applications. The damage caused by mechanical actions during the installation and the
83 chemical and the biological degradation are important issues to be considered in the

84 behaviour of these materials. The changes in their physical, mechanical and hydraulic
85 properties, induced by these degradation processes, can compromise the performance of
86 the structures where these materials are used.

87 The available long-term tensile strength of a geosynthetic (AASHTO, 2012; FHWA,
88 2010), T_{al} , or the design strength for the ultimate limit state (BS 8006, 2010), can be
89 estimated as:

$$T_{al} = \frac{T_{ult}}{RF_{ID} \times RF_{CR} \times RF_D} \quad (1)$$

91 where T_{ult} is the ultimate tensile strength (per unit width) determined according to the
92 standards (ASTM D6637 - 11; ASTM D 4595; EN ISO 10319), RF_{ID} is the installation
93 damage reduction factor (that accounts for the damaging effects of placement and
94 compaction of soil or aggregate over the geosynthetic during installation), RF_{CR} is the
95 creep reduction factor (that accounts for the effect of creep resulting from long-term
96 sustained tensile load applied to the geosynthetic) and RF_D is the durability reduction
97 factor (that accounts for the strength loss caused by chemical and biological degradation
98 of the polymers used in the geosynthetic). Instead of the durability reduction factor,
99 RF_D , the British Standard (BS 8006, 2010) considers two reduction factors: a reduction
100 factor for weathering, RF_w , and a reduction factor for chemical/environmental effects,
101 RF_{CH} .

102 Over the last years several field studies regarding the installation damage of
103 geosynthetics have been performed (Hufenus et al., 2005; Lim and McCartney, 2013;
104 Pinho-Lopes and Lopes, 2014; Troost and Ploeg, 1990; Watts and Brady, 1990, 1994).
105 They have shown that the type of geosynthetic, the weight, type and number of passes

106 of the compaction material, the gradation and angularity of the fill influence the level of
107 damage. The results presented by Watts and Brady (1990) revealed that the tensile
108 strength and the elongation at break were both substantially reduced by the damage
109 during installation but the Young's modulus was largely unaffected. Troost and Ploeg
110 (1990) also found that the shape of the load-strain curve remains almost identical after
111 installation damage, provided that not too many yarns were broken. More recently, the
112 results reported by Hufenus et al. (2005) have also shown that the slope of the load-
113 strain curve was not largely affected by the installation damage even when the
114 maximum tensile strength and elongation at break decreased.

115 Based on data from controlled installation damage trials reported in the literature,
116 Allen and Bathurst (1994) concluded that the initial modulus of the load-strain curves
117 may or may not be shifted and the modulus of some materials does not change and in
118 some cases appears to be slightly greater after exhumation.

119 Chemical and biological degradation has been studied mainly on geosynthetics used
120 in landfill barrier systems. A review on the degradation and field long-term of HDPE
121 geomembranes was presented by Rowe and Sangam (2002). Based on examination of
122 both laboratory and field data, Rowe and Sangam (2002) have concluded that the
123 projected service lives of HDPE geomembranes may range from many centuries to less
124 than a decade, depending on the material and exposure conditions.

125 The oxidation degradation of geosynthetic in field conditions is affected by the
126 temperature, oxygen partial pressure and chemical constituents of the surround media
127 (pH, transition metal ions, etc.) (Hsuan et al., 2008). Temperature plays the most critical
128 role of all physical and chemical processes. The oxidation mechanism is governed by

129 the transport processes of oxygen which are all strongly temperature dependent. The
130 available oxygen concentration in the environment surrounding the geosynthetic is
131 essential to the degradation by oxidation. Different oxidation reactions can take place
132 based on the available oxygen, however the reaction rate at ambient temperature is very
133 slow (Hsuan et al., 2008). The oxidation of polyolefins (like polypropylene) can be
134 accelerated by the presence of transition metal ions such as cobalt manganese, copper,
135 and iron while the oxidation degradation of a polypropylene geotextile can be
136 accelerated by the presence of rusting steel wires (Hsuan et al., 2008).

137 The resistance of a non-woven polypropylene needle punched geotextile against
138 some degradation agents, such as liquids, thermo-oxidation and artificial weathering,
139 and the existence of synergisms between them was studied by Carneiro et al. (2014)
140 through laboratory tests. These authors found that the thermo-oxidative resistance was
141 affected by sodium hydroxide and iron nitrate.

142 According to Koerner et al. (2007) biological degradation of geosynthetics is
143 generally not a factor of concern unless biologically sensitive additives (such as low-
144 molecular-weight plasticizers) are included in the polymer formulation.

145 In order to study the chemical and biological degradation induced by recycled
146 C&DW on two geosynthetics, a damage trial embankment (2m x 3m in plant) was
147 constructed. This trial damage embankment intends to simulate the potential
148 degradation induced by recycled C&DW on the tensile behaviour of two geosynthetics
149 with different structure and base polymers. Its construction method and dimensions are
150 not adequate for other purposes, namely the analysis of the embankment behaviour. It
151 was predicted the exhumation of geosynthetic samples from the embankment after 6, 12

152 and 24 months of its construction. The results herein presented are related to the
153 samples exhumed after 6 months of construction.

154 Notwithstanding the fact that the period of time between the installation and the
155 exhumation of the geosynthetic specimens are not equivalent or comparable to the
156 service life of the structures, the construction of this trial embankment will allow us to
157 have an estimate of the degradation level, induced by the environmental conditions in
158 which the geosynthetics were inserted, on their short-term tensile behaviour.

159

160 **2. MATERIALS AND METHODS**

161 *2.1. Geosynthetics*

162 Two commercial available geosynthetics frequently used as reinforcement were used
163 in this study: an extruded uniaxial high density polyethylene (HDPE) geogrid (Figure
164 1a) and a high-strength composite geotextile consisting of polypropylene continuous-
165 filament needle-punched nonwoven and high-strength polyester yarns (unidirectional
166 geocomposite reinforcement) (Figure 1b). Table 1 summarizes the main properties of the
167 geosynthetics provided by the manufacturers.

168 To analyse the effects of recycled C&DW on the short-term tensile behaviour of
169 these geosynthetics, intact (as supplied by the manufacturers) and exhumed specimens
170 were taken from the same roll and they were tested using the same methods and
171 equipments.

172 The tensile tests were carried out in accordance with the European Standard EN ISO
173 10319 (2008) on five specimens (intact or exhumed) and with strain rate of 20%/min.

174 The preparation of the geocomposite specimens to perform tensile tests needs some
175 previous work, namely the use of a particular nitrile based adhesive to glue the polyester
176 yarns in the portion of geotextile located inside the clamps and the placement of steel
177 rods of small diameter to avoid the sliding of the geotextile during the tests (Figure 2).

178 Each geocomposite specimen was cut with dimensions 200 mm width × 340 mm
179 length. The distance between the jaws was adjusted to give a test specimen length of
180 100 mm. The reference points were fixed on the specimens 60 mm apart. A video-
181 extensometer was used to measure the geosynthetic strains.

182 The geogrid specimens were cut with a width of 200 mm (9 longitudinal bars) and
183 length of 470 mm. The distance between the clamps was adjusted to give a test
184 specimen length of 395 mm approximately, to ensure fixing the geogrid on the
185 transversal bars. The reference points for the video-extensometer were fixed on the
186 specimens 200 mm apart.

187

188 2.2. Recycled C&DW

189 The trial damage embankment was constructed using a fine grain recycled C&DW,
190 coming mainly from the demolition of single-family houses and cleaning of lands with
191 illegal deposition of C&DW, provided by a Portuguese Recycling plant located in
192 Centre region. The constituents of the C&DW determined in accordance with the
193 European Standard EN 933-11 (2009) are listed in Table 2. The predominant materials
194 of this recycled C&DW are concrete, mortar, unbound aggregates and natural stones. A
195 significant amount of soils was also identified. The volume of floating particles exceeds

196 the desirable value ($< 5\text{cm}^3/\text{kg}$), meaning that some wood and polystyrene is present in
197 the recycled material.

198 The gradation of the recycled C&DW was determined following the European
199 Standard EN 933-1 (2009) for aggregates. It was observed that the oven drying at 110°C
200 caused the melting and merging of some particles, so it was necessary to use the
201 procedure described in Annex B of the Standard to determine the initial weight of the
202 sample. The particle size distribution, obtained by sieving, is represented in Figure 3.

203 The environmental concerns regarding the potential contamination of the
204 groundwater, as well as, the possible presence of substances that could induce
205 geosynthetics degradation, impose the evaluation of the leaching behaviour of the
206 recycled waste. Thus, laboratory leaching tests were carried out in accordance with the
207 European Standard EN 12457-4 (2002).

208 Table 3 presents the leaching test results and the acceptance criteria for leached
209 maximum concentration for inert landfill, define by the European Council Decision
210 2003/33/EC (2003).

211 From the analysis of the results presented in Table 3 it can be concluded that only the
212 value of sulphate exceeds the maximum value established by the European legislation,
213 notwithstanding the Directive 2003/33/EC (Council Decision 2003/33/EC) states that “*if*
214 *the waste does not meet these values for sulphate, it may still be considered as*
215 *complying with the acceptance criteria if the leaching does not exceed 6000 mg/kg at*
216 *L/S = 10 l/kg, determined either by a batch leaching test or by a percolation test under*
217 *conditions approaching local equilibrium.*”

218 The alkaline pH value can induce some chemical degradation on the geosynthetics,
219 however since the pH is within the range 3 – 9 (and the maximum dimension does not
220 exceed 19mm), the fill material could be classified, in accordance with AASHTO,
221 (2012), as non-aggressive.

222

223 2.3. Embankment construction

224 The damage trial embankment was constructed with dimensions in plan of 2m × 3m
225 and height of 0.45 m. Inside the embankment, 8 geogrid samples (0.45 m × 1.5m) and 8
226 geocomposite samples (0.47 × 1.5m) were distributed in 2 levels, vertically spaced of
227 0.20 m.

228 After cleaning the foundation from the existing vegetation (Figure 4a), a 0.05m high
229 layer was placed and compacted. Eight geosynthetic samples (4 geogrid samples and 4
230 geocomposite samples) were carefully positioned without overlapping. Geosynthetic
231 samples were covered with a first layer of C&DW placed manually to prevent
232 mechanical damage (Figure 4b). Then additional quantities of C&DW were disposed,
233 evenly spread and compacted to reach a lift with final thickness of 0.20 m.

234 The compaction was performed with a forward compaction plate with weight of
235 94 kg, plate dimensions of 450 mm x 696 mm, static pressure of 382 kg/m² and
236 optimum vibration force of 16.5kN at 92Hz (Figure 4c).

237 A second layer of geosynthetic samples (4 geogrid samples and 4 geocomposite
238 samples) was positioned and the same steps were repeated to reach a lift with final
239 thickness of 0.20 m.

240 The lateral slopes of the embankment were also compacted with the forward
241 compaction plate and aggregates from recycled C&DW were deposited to prevent
242 erosion by rain water (Figure 4d).

243 A lightweight compaction process was adopted in order to minimize the installation
244 damage of the geosynthetics. Field evaluations performed by Richardson (1998) have
245 shown that installation damage can be minimized by using a minimum 250 mm initial
246 lift over the geosynthetic and by limiting the maximum stone size to less than 25% of
247 the lift thickness. In this trial embankment the final thickness of the layers placed over
248 the geosynthetics is equal to 0.20 m, but the maximum particle size of the recycled
249 C&DW is 18 mm, significantly lower than 25% of the lift thickness.

250

251 *2.4. Specimens exhumation*

252 After 6 months of the trial embankment construction, the first samples were carefully
253 exhumed to prevent additional damage. Four geosynthetic samples (2 geogrid samples
254 and 2 geocomposite samples) were exhumed from the upper layer.

255 The exhumation began with the removal of the aggregates placed on the lateral
256 slopes of the embankment, as well as, the vegetation that grew up over the embankment
257 (Figure 5a). Then the fill material was manually removed with hoes and shovels until
258 reaching the geosynthetics (Figure 5b), being the material just above the geosynthetics
259 removed carefully with the hands (Figure 5c).

260 From the visual inspection, the geogrid did not show significant damages (visible to
261 the naked eye). Geocomposite samples were damaged by plant roots that crossed the
262 geotextile, some of them with a few millimetres in diameter (Figure 5d). The exhumed

263 samples were put into plastic bags and transported to the laboratory where they
264 remained at 20°C until be tested.

265 After the exhumation of the samples, the recycled C&DW was replaced and
266 compacted by similar process used in the construction, so that resembling conditions for
267 the remained samples were maintained.

268

269 **3. RESULTS AND DISCUSSION**

270 *3.1. SEM images*

271 As mentioned in 2.4, the preliminary visual inspection of the exhumed samples did
272 not reveal significant damages, apart from the plant roots that crossed the base
273 geotextile of the geocomposite. In order to evaluate the damages with more detail,
274 Scanning Electron Microscope (SEM) analyses were carried out.

275 The SEM analyses were performed using a High resolution Environmental Scanning
276 Electron Microscope with X-Ray Microanalysis and Electron Backscattered Diffraction
277 analysis (Quanta 400 FEG ESEM / EDAX Genesis X4M) from the Materials Centre of
278 University of Porto.

279 Figure 6 shows SEM images (at ×500 magnification) of the longitudinal bars of the
280 geogrid took from an intact specimen and an exhumed specimen. Only very small
281 cavities and grooves were detected, appearing to be provoked by hard particles of the
282 recycled C&DW.

283 SEM images of intact and exhumed specimens of geocomposite are illustrated in
284 Figure 7. Figure 7(b) shows that fibres fixing the PET yarns to the base geotextile are
285 still present even if they seem to be unrolled. Figure 7(c) and 7(d) show amplified

286 images of the base nonwoven geotextile. Since the holes provoked by the plant roots are
287 local damages visible to the naked eye, the specimens for SEM analyses (with diameter
288 of 25 mm) were cut from a more representative area.

289 It is possible to see that some fibres of the geotextile are damaged in the exhumed
290 specimen (Figure 7d). Images from PET yarns (Figure 7e and 7f) did not reveal
291 significant damage on exhumed specimens. Very small particles are held to the yarns.

292 The images presented in Figure 6 and Figure 7 allow us to conclude that, as intended,
293 the installation damage (induced by the construction process) was not very significant.

294

295 3.2. Tensile tests

296 Figure 8 presents load-strain curves of intact geogrid and exhumed geogrid
297 specimens subjected to tensile tests carried out according to EN ISO 10319 (2008). It
298 would be expected that the variability of the results for exhumed specimens would be
299 greater than that of intact specimens, due to the different mechanisms that could
300 contribute to the geosynthetics damage. However the results presented in Figure 8 and
301 summarised in Table 4 and Table 5 contradict this assumption. In fact tensile tests
302 carried out with intact geogrid specimens have shown great variability, even so the
303 coefficient of variation for the tensile strength was smaller than 4.2%. This variability is
304 usual and it might be attributed to the production process.

305 Table 4 and Table 5 present the maximum tensile strength (T_{max}), the geosynthetic
306 strain for T_{max} ($\epsilon_{T_{max}}$), the secant stiffness modulus at strain of 2% ($J_{2\%}$) and the secant
307 stiffness modulus at $\epsilon_{T_{max}}$ ($J_{T_{max}}$) for intact and exhumed geogrid specimens,
308 respectively. The mean values of these parameters and the 95% confidence intervals

309 assuming a Student's t-distribution were also included. The Student's t-distribution was
310 assumed since the population standard deviation is unknown and the number of
311 specimens is lower than 30.

312 The mean value of the tensile strength for exhumed specimens is outside the
313 confidence interval of this parameter for intact specimens. Even if the lowest value of
314 the tensile strength achieved in an intact specimen (Table 4) is coincident to the highest
315 value recorded in exhumed specimens (Table 5), one can conclude that the C&DW
316 induced the decrease of the geogrid tensile strength and stiffness modulus and the
317 increase of peak strain (ϵ_{Tmax}).

318 Figure 9 compares the mean load-strain curve for intact specimens with the mean
319 load-strain curve for the exhumed specimens. The shape of the curves for intact and
320 exhumed specimens are similar but the coordinates at failure were shifted. The geogrid
321 stiffness for very small strains (initial stiffness) did not change significantly but the
322 secant modulus reduced. One can conclude that the recycled C&DW induced a small
323 decrease on the geogrid tensile strength (5.9% on average) and the reduction of the
324 geogrid stiffness.

325 Load-strain curves for intact and exhumed geocomposite (high strength geotextile)
326 specimens are presented in Figure 10. As expected, the scattering of the results is more
327 pronounced in exhumed specimens. The behaviour of Specimen 4 can be partly
328 explained by local damage induced by plant roots (Figure 5d). Table 6 and Table 7
329 summarise the results of tensile tests carried out on intact and exhumed geocomposite
330 specimens, respectively. The 95% confidence intervals assuming a Student's t-
331 distribution are also presented.

332 The recycled C&DW induced the reduction of the geocomposite tensile strength
333 (16% on average) but the effect on the geocomposite tensile stiffness is not significant
334 (Figure 11). The decrease on the secant stiffness modulus at ϵ_{Tmax} (J_{Tmax}) is obvious
335 since the geocomposite fails for smaller strains. The shape of curves for intact and
336 exhumed specimens are quite similar.

337 The high tensile stiffness of this geocomposite (when compared to other geotextiles)
338 results mainly from the high modulus of polyester (PET) yarns. Visual inspection and
339 SEM images (Figure 7f) did not reveal significant damage in PET yarns, although some
340 damage produced by plant roots (Figure 5d) and other installation damage mechanisms
341 (Figure 7d) on nonwoven geotextile could be identified. The degradation of the
342 nonwoven geotextile (base of the geocomposite) could explain the reduction of the
343 geocomposite tensile strength without significant change of the geocomposite stiffness
344 modulus until failure (Figure 11).

345 The retained values of relevant parameters to characterise the load-strain behaviour,
346 such as the tensile strength, the strain at maximum load or the secant stiffness modulus,
347 are frequently used to quantify the damage on geosynthetics. The retained value of a
348 generic parameter, X, is defined as:

$$R_X = \frac{X_{dam}}{X_{intact}} \quad (2)$$

350 where X_{dam} is the value of parameter X for damaged (or exhumed) specimens and
351 X_{intact} is the value for intact specimens. By definition, the mean value of R_X is not
352 simply the ratio of the mean of populations X_{dam} and X_{intact} , as is typically presented in
353 the literature (Mood et al., 1974). The mean value of R_X is the mean value of the

354 quantities R_X estimated by equation (1). In this paper, the retained tensile strength, R_T ,
355 the retained peak strain, R_ϵ , and the retained secant modulus at 2% of strain, $R_{J2\%}$, were
356 estimated to characterise the damage induced by recycled C&DW on the geosynthetics
357 under analysis.

358
359 Table 8 summarises the mean values of R_T , R_ϵ , and $R_{J2\%}$ estimated as the ratio
360 between the mean value of the parameter (tensile strength, peak strain or secant
361 modulus) for exhumed specimens and the corresponding mean value for intact
362 specimens ($\bar{X}_{\text{dam}}/\bar{X}_{\text{intact}}$), as well as, as the mean value of the 25 possible
363 combinations to estimate R_X by equation (2) ($\overline{\bar{X}_{\text{dam}}/\bar{X}_{\text{intact}}}$). The values were
364 presented with three decimal digits to demonstrate the reduced differences between the
365 values estimated by the two approaches. In fact, the error is small if R_X is estimated as
366 the ratio of the mean values. This finding can be justified by the low variability of the
367 results.

368 The data indicates that the effect of the C&DW on the short-term tensile behaviour
369 of the geosynthetics depends on the structure and base polymer of the material. The loss
370 of strength was more pronounced in the geocomposite, notwithstanding no reduction in
371 the secant modulus was recorded for this material. In the geogrid, the loss of strength on
372 exhumed specimens was similar to the loss of stiffness at 2% of strain. The peak strain
373 increased resulting in a more pronounced loss of stiffness at failure (retained secant
374 stiffness modulus of 0.89).

375 The lack of change in the stiffness modulus observed in the geocomposite was also
376 reported by Allen and Bathurst (1994) and Watts and Brady (1990) in installation

377 damage trials for structurally simple geosynthetics (woven geotextiles and geogrids).
378 Allen and Bathurst (1994) have justified this evidence by local defects induced in the
379 geosynthetic that causes premature failure in the fibers/yarns at reduced strains.

380 The unchanged tensile stiffness modulus observed on the geocomposite suggests that
381 after 6 months of exposure the damage induced in the polyester yarns could be
382 neglected, even if some damaged was observed in the base geotextile (Figure 5d and
383 Figure 7d).

384

385 **4. CONCLUSIONS**

386 The main objective of this paper is the characterisation of the changes in load-strain
387 behaviour of two geosynthetics used as reinforcement material (a uniaxial high density
388 polyethylene geogrid and a high-strength composite geotextile) due to the potential
389 degradation induced by a recycled C&DW.

390 SEM images allow us to conclude that the installation damage (induced by the
391 construction process) was not very significant. Visual inspection and SEM images did
392 not reveal significant damage in PET yarns of the geocomposite, although some damage
393 produced by plant roots on the nonwoven geotextile (base of the geocomposite) could
394 be identified.

395 The results of tensile tests carried out on intact and exhumed specimens indicate that
396 the effects of the C&DW on the short-term load-strain behaviour of the geosynthetics
397 depend on the structure and base polymer of the material. On the HDPE geogrid the
398 recycled C&DW induced a small decrease on the geogrid tensile strength and the
399 reduction of the geogrid tensile stiffness. The recycled C&DW induced the reduction of

400 the geocomposite tensile strength (16% on average) but the effect on the geocomposite
401 tensile stiffness is not significant. The shape of the load-strain curves for intact and
402 exhumed specimens are, on average, quite similar.

403 It should be pointed out that the results and conclusions herein presented are
404 preliminary results, since they are related to the exhumation of the specimens after 6
405 months of the trial embankment construction. Broadening conclusions will be reached
406 when possible the exhumation of specimens submitted to longer periods of exposure.

407

408 **ACKNOWLEDGMENTS**

409 The authors would like to thank the financial support of Portuguese Science and
410 Technology Foundation (FCT) and FEDER, through the Research Project: FCOMP-01-
411 0124-FEDER-028842, RCD-VALOR – Sustainable application of Recycled
412 Construction and Demolition Wastes (C&DW) in geosynthetics reinforced structures
413 (PTDC/ECM-GEO/0622/2012). The authors also thank Tensar International and
414 TenCate Geosynthetics Iberia for providing the geosynthetics used in this study and
415 RCD, SA for making facilities available to construct the trial embankment.

416

417 **REFERENCES**

418 AASHTO, 2012. LRFD Bridge Design Specifications, 3rd Edition, Washington DC.
419 Allen, A.M., Bathurst, R.J., 1994. Characterization of geosynthetic load-strain
420 behaviour after installation damage. Geosynthetics International 1, 181-199.

421 Arulrajah, A., Piratheepan, J., Disfani, M.M., Bo, M.W., 2013a. Geotechnical and
422 Geoenvironmental Properties of Recycled Construction and Demolition Materials in
423 Pavement Subbase Applications. *Journal of Materials in Civil Engineering* 28, 1077-
424 1088.

425 Arulrajah, A., Rahman, M.A., Piratheepan, J., Bo, M.W., Imteaz, M.A., 2013b.
426 Interface Shear Strength Testing of Geogrid-Reinforced Construction and Demolition
427 Materials. *Advances in Civil Engineering Materials* 2, 189 - 200.

428 ASTM D 4595, 2011. Standard test method for tensile properties of geotextiles by
429 the wide-width strip method, American Society for Testing Materials, USA.

430 ASTM D6637 - 11, 2011. Standard Test Method for Determining Tensile Properties
431 of Geogrids by the Single or Multi-Rib Tensile Method, American Society for Testing
432 Materials, USA.

433 BS 8006, 2010. Code of practice for strengthened/reinforced soils and other fills,
434 British Standard Institution.

435 Carneiro, J.R., Almeida, P.J., Lopes, M.L., 2014. Some synergisms in the laboratory
436 degradation of a polypropylene geotextile. *Construction and Building Materials* 73,
437 586–591.

438 Council Decision 2003/33/EC, 2003. Council Decision establishing criteria and
439 procedures for the acceptance of waste at landfills pursuant to Article 16 of and Annex
440 II to Directive 1999/31/EC. *Official Journal of European Union* L11/27.

441 EN 12457-4, 2002. Characterisation of waste - Leaching - Compliance test for
442 leaching of granular waste materials and sludges - Part 4: One stage batch test at liquid

443 to solid ratio of 10l/kg for materials with particle size below 10 mm (without or with
444 size reduction), CEN.

445 EN 933-1, 2009. Tests for geometrical properties of aggregates - Part 1:

446 Determination of particle size distribution - Sieving method. CEN.

447 EN 933-11, 2009. Tests for geometrical properties of aggregates - Part 11:

448 Classification test for the constituents of coarse recycled aggregate. CEN.

449 EN ISO 10319, 2008. Geosynthetics - Wide width tensile test, International

450 Organization for Standardization, TC 221.

451 FHWA, 2010. Design and Construction of Mechanically Stabilized Earth Walls and

452 Reinforced Soil Slopes, in: Berg, R.R., Christopher, B.R., Samtani, N.C. (Eds.),

453 FHWA-NHI-10-024 Washington D.C.

454 Hsuan, Y.G., Schroeder, H.F., Rowe, K., Müller, W., Greenwood, J., Cazzuffi, D.,

455 Koerner, R.M., 2008. Long-term performance and lifetime prediction of geosynthetics,

456 Proc. 4th European Geosynthetics Conference, Edinburgh, September 2008, Keynote

457 Paper.

458 Hufenus, R., Ruegger, R., Flum, D., Sterba, I.J., 2005. Strength reduction factors due

459 to installation damage of reinforcing geosynthetics. Geotextiles and Geomembranes 23,

460 401–424.

461 Jiménez, J. R., Ayuso, J., Agrela, F., López, M., & Galvín, A. P. (2012). Utilisation

462 of unbound recycled aggregates from selected CDW in unpaved rural roads. Resources,

463 Conservation and Recycling, 58(0), 88-97.

464 Koerner, G.R., Hsuan, Y.G., Koerner, R.M., 2007. The durability of geosynthetics,
465 in: Sarsby, R.W. (Ed.), Geosynthetics in Civil Engineering. Woodhead publishing
466 Limited and CRC Press.

467 Lim, S.Y., McCartney, J.S., 2013. Evaluation of effect of backfill particle size on
468 installation damage reduction factors for geogrids. Geosynthetics International 20, 62–
469 72.

470 Mood, A.M., Graybill, F.A., Boes, D.C., 1974. Introduction to the Theory of
471 Statistics, 3rd Edition. McGraw-Hill, New York.

472 Pinho-Lopes, M., Lopes, M.L., 2014. Tensile properties of geosynthetics after
473 installation damage. Environmental Geotechnics 1, 161-178.

474 Rahman, M. A., Arulrajah, A., Piratheepan, J., Bo, M. W., & Imteaz, M. A. (2013).
475 Resilient Modulus and Permanent Deformation Responses of Geogrid-Reinforced
476 Construction and Demolition Materials. Journal of Materials in Civil Engineering.

477 Rahman, M. A., Imteaz, M. A., Arulrajah, A., Piratheepan, J., & Disfani, M. M.
478 (2015). Recycled Construction and Demolition materials in permeable pavement
479 systems: Geotechnical and hydraulic characteristics. Journal of Cleaner Production, 90,
480 183-194.

481 Richardson, G.N., 1998. Field evaluation of geosynthetic survivability in aggregate
482 road base. Geotechnical Fabrics Report, September.

483 Rowe, R.K., Sangam, H.P., 2002. Durability of HDPE geomembranes. Geotextiles
484 and Geomembranes 20, 77–95.

485 Troost, G.H., Ploeg, N.A., 1990. Influence of weaving structure and coating on the
486 degree of mechanical damage of reinforcing mats and woven geogrids caused by

This manuscript is the accepted version of the paper:

Damage induced by recycled Construction and Demolition Wastes on the short-term tensile behaviour of two geosynthetics, Transportation Geotechnics, Vol.4, pp. 64-75, DOI: [10.1016/j.trgeo.2015.07.002](https://doi.org/10.1016/j.trgeo.2015.07.002)

487 different fills during installation, Fourth International Conference on Geotextiles,

488 Geomembranes and Related Products, Den Haag, pp. 609-614.

489 Watts, G.R.A., Brady, K.C., 1990. Site damage trials on geotextiles, Fourth

490 International Conference on Geotextiles, Geomembranes and Related Products, Den

491 Haag, pp. 603-607.

492 Watts, G.R.A., Brady, K.C., 1994. Geosynthetics - installation damage and the

493 measurement of tensile strength, Fifth International Conference on Geotextiles,

494 Geomembranes and Related Products, Singapore, pp. 1159-1164.

495

496

497

498

499

500

501

502

503

504

Accepted Version

505

506

507

TABLES

508

509 Table 1. Properties of the geosynthetics provided by manufacturers.

	Geogrid	Geotextile
Raw material	HDPE	PP & PET
Unit weight (g/m ²)	450	340
Aperture dimensions (mm)	16×219	-
Mean value of the tensile strength (kN/m)	68	75/14 [#]
Elongation at maximum load (%)	11±3	10

510

[#] Machine direction / Cross direction.

511

512

513

514

515

516

517

518

519

520

521

522

523

524

525 Table 2. Classification of recycled C&DW constituents.

Constituents	
Concrete, concrete products, mortar, concrete masonry units, R_c (%)	36.8
Unbound aggregate, natural stone, hydraulically bound aggregate, R_u (%)	33.7
Clay masonry units, calcium silicate masonry units, aerated non-floating concrete, R_b (%)	10.8
Bituminous materials, R_a (%)	0.5
Glass, R_g (%)	1.0
Soils, R_s (%)	17.1
Other materials, X (%)	0.1
Floating particles, FL (cm^3/kg)	7.80

526

527

528

529

530

531

532

533

534

535

536

537

538

539

540

541

542 Table 3. Leaching test results.

Parameter	Value (mg/kg)	Acceptance criteria for leached concentrations – Inert landfill
Arsenic, As	0.013	0.5
Lead, Pb	< 0.01	0.5
Cadmium, Cd	< 0.003	0.04
Chromium, Cr	< 0.01	0.5
Copper, Cu	0.029	2
Nickel, Ni	0.01	0.4
Mercury, Hg	< 0.002	0.01
Zinc, Zn	< 0.1	4
Barium, Ba	0.069	20
Molybdenum, Mo	0.036	0.5
Antimony, Sb	0.011	0.06
Selenium, Se	< 0.02	0.1
Chloride, Cl	19	800
Fluoride, F	< 1.5	10
Sulphate, SO ₄	2100	1000
Dissolved Organic Carbon, DOC	25	500
Dissolved Solids, DS	3030	4000
pH	8.3	-

543

544

545

546

547

548

549

550

551

552

553 Table 4. Summary of results of tensile tests carried out on intact geogrid specimens.

	T_{\max} (kN/m)	$\epsilon_{T_{\max}}$ (%)	$J_{2\%}$ (kN/m)	$J_{T_{\max}}$ (kN/m)
Specimen 1	63.6	10.4	1144	612
Specimen 2	57.8	9.8	1074	593
Specimen 3	58.8	10.4	1063	564
Specimen 4	62.2	9.8	1149	638
Specimen 5	58.9	10.2	996	578
Mean value	60.3	10.1	1085	597
Confidence interval of 95%	60.3 ± 3.1	10.1 ± 0.4	1085 ± 79	597 ± 36

554

555

556

557

558

559

560

561

562

563

564

565

566

567

568

569

570

571

572

573 Table 5. Summary of results of tensile tests carried out on exhumed geogrid
574 specimens.

	T_{\max} (kN/m)	$\epsilon_{T_{\max}}$ (%)	$J_{2\%}$ (kN/m)	$J_{T_{\max}}$ (kN/m)
Specimen 1	55.5	10.3	988	539
Specimen 2	57.0	10.9	1008	524
Specimen 3	57.4	10.7	1026	538
Specimen 4	55.8	10.7	1015	522
Specimen 5	57.8	10.6	1024	544
Mean value	56.7	10.6	1012	534
Confidence interval of 95%	56.7 ± 1.2	10.6 ± 0.3	1012 ± 19	534 ± 12

575

576

577

578

579

580

581

582

583

584

585

586

587

588

589

590

591

592 Table 6. Summary of results of tensile tests carried out on intact geocomposite
593 specimens.

	T_{\max} (kN/m)	$\epsilon_{T_{\max}}$ (%)	$J_{2\%}$ (kN/m)	$J_{T_{\max}}$ (kN/m)
Specimen 1	70.1	9.2	693	765
Specimen 2	67.6	10.0	605	676
Specimen 3	73.7	10.7	648	691
Specimen 4	69.0	9.7	742	714
Specimen 5	72.7	9.2	549	793
Mean value	70.6	9.7	647	728
Confidence interval of 95%	70.6 ± 3.2	9.7 ± 0.8	647 ± 93	728 ± 62

594

595

596

597

598

599

600

601

602

603

604

605

606

607

608

609

610

611 Table 7. Summary of results of tensile tests carried out on exhumed geocomposite
612 specimens.

	T_{\max} (kN/m)	$\epsilon_{T_{\max}}$ (%)	$J_{2\%}$ (kN/m)	$J_{T_{\max}}$ (kN/m)
Specimen 1	65.8	9.3	673	704
Specimen 2	60.5	8.3	844	726
Specimen 3	57.5	8.5	604	673
Specimen 4	51.3	9.4	442	548
Specimen 5	61.3	9.0	647	684
Mean value	59.3	8.9	642	667
Confidence interval of 95%	59.3 ± 6.7	8.9 ± 0.6	642 ± 126	667 ± 61

613

614

615

616

617

618

619

620

621

622

623

624

625

626

627

628

629

630 Table 8. Mean values of retained tensile strength, R_T , retained peak strain, R_ϵ , and
631 retained secant modulus, $R_{J2\%}$.

	Geogrid			Geocomposite		
	R_T	R_ϵ	$R_{J2\%}$	R_T	R_ϵ	$R_{J2\%}$
Estimated as $\bar{X}_{\text{dam}}/\bar{X}_{\text{intact}}$	0.941	1.052	0.933	0.839	0.915	0.992
Estimated as $\overline{X_{\text{dam}}/X_{\text{intact}}}$	0.942	1.053	0.936	0.840	0.918	1.003

632

633

634

635

636

637

638

639

640

641

642

643

644

645

646

647

648

649

650

Accepted Version

651 **LIST OF FIGURES**

652 Figure 1 – Visual aspect of intact geosynthetics (ruler in centimetres): a) uniaxial
653 HDPE geogrid; b) high-strength composite geotextile (geocomposite).

654
655 Figure 2 - Some stages of geocomposite specimens preparation for tensile tests.

656
657 Figure 3 - Particle size distribution of the Recycled C&DW used in the trial
658 embankment.

659
660 Figure 4 - Trial embankment construction: a) cleaning of the foundation; b) manual
661 placement of the C&DW over the geosynthetics; c) compaction of the final layer;
662 d) lateral protection of the slopes with aggregates from C&DW.

663
664 Figure 5 - Specimens exhumation: a) removal of vegetation and lateral aggregates;
665 b) geogrid appearing during exhumation; c) careful exhumation of the specimens;
666 d) plant roots crossing the geotextile.

667
668 Figure 6 – SEM images of the longitudinal bars of the geogrid (×500): a) intact
669 specimen; b) exhumed specimen after 6 months.

670
671 Figure 7 – SEM images of geocomposite specimens: a) intact (×50); b) exhumed
672 specimen (×50); c) intact (×500); d) exhumed specimen (×500); e) intact (×1000);
673 f) exhumed specimen (×1000).

674
675 Figure 8 – Load-strain curves of tensile tests performed on: a) intact geogrid
676 specimens; b) exhumed geogrid specimens.

677
678 Figure 9 – Comparison of load-strain curves of intact and exhumed geogrid
679 specimens.

680
681 Figure 10 – Load-strain curves of tensile tests performed on: a) intact geocomposite
682 specimens; b) exhumed geocomposite specimens.

683
684 Figure 11 – Comparison of load-strain curves of intact and exhumed geocomposite
685 specimens.

686
687

688

689

690

FIGURES

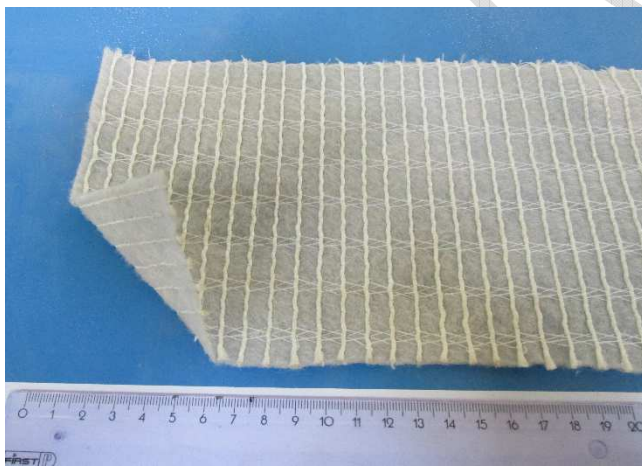
691



692

693

(a)



694

695

(b)

696

Figure 1 – Visual aspect of intact geosynthetics (ruler in centimetres): a) uniaxial

697

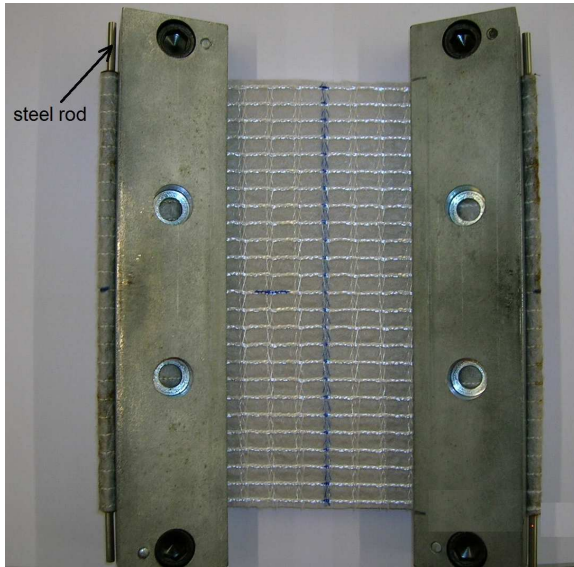
HDPE geogrid; b) high-strength composite geotextile (geocomposite).

698

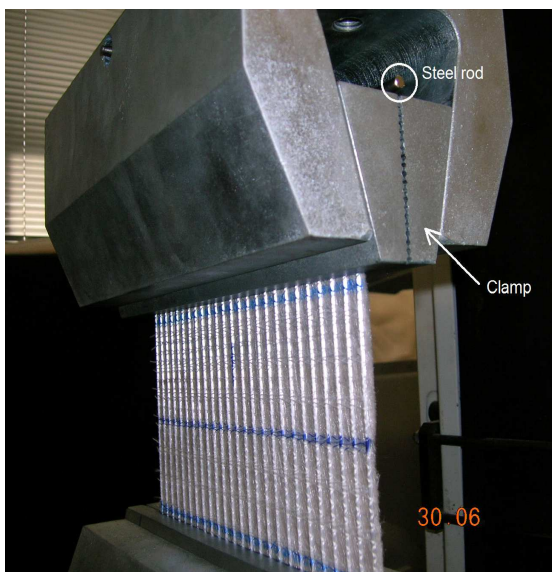
699

700

701



702



703

704 Figure 2 - Some stages of geocomposite specimens preparation for tensile tests.

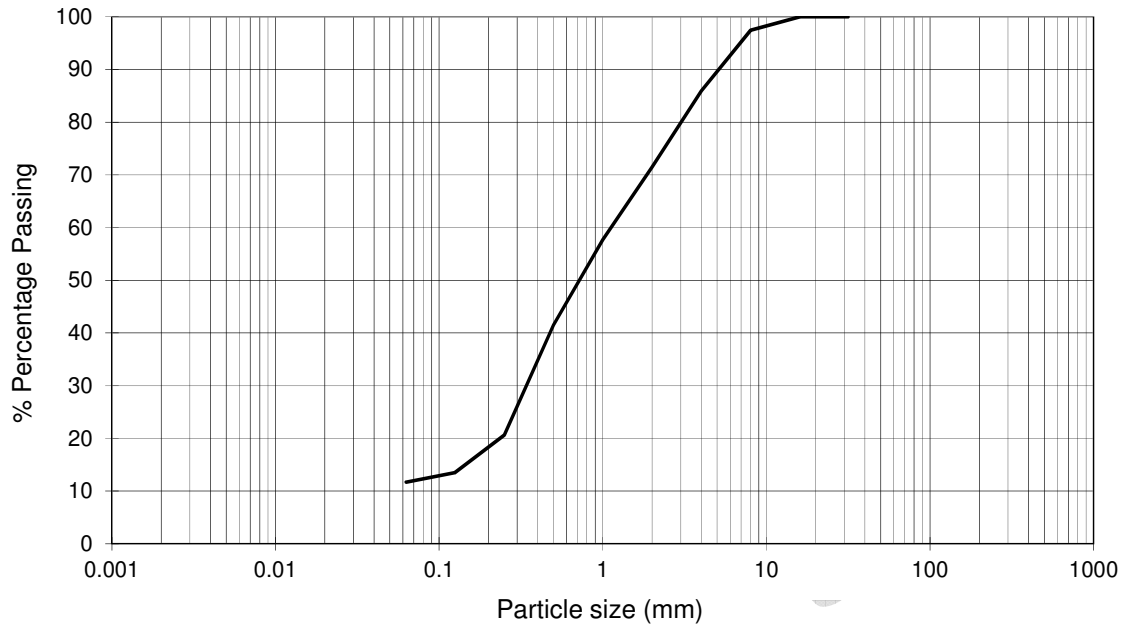
705

706

707

708

709



710

711 Figure 3 - Particle size distribution of the Recycled C&DW used in the trial

712 embankment.

713

714

715

716

717

718

719

720

721

722

723

724

725



(a)

(b)



(c)

(d)

726

727 Figure 4 - Trial embankment construction: a) cleaning of the foundation; b) manual

728 placement of the C&DW over the geosynthetics; c) compaction of the final layer; d)

729 lateral protection of the slopes with aggregates from C&DW.

730

731

732

733

734



(a)

(b)



(c)

(d)

735

736 Figure 5 - Specimens exhumation: a) removal of vegetation and lateral aggregates; b)

737 geogrid appearing during exhumation; c) careful exhumation of the specimens; d) plant

738 roots crossing the geotextile.

739

740

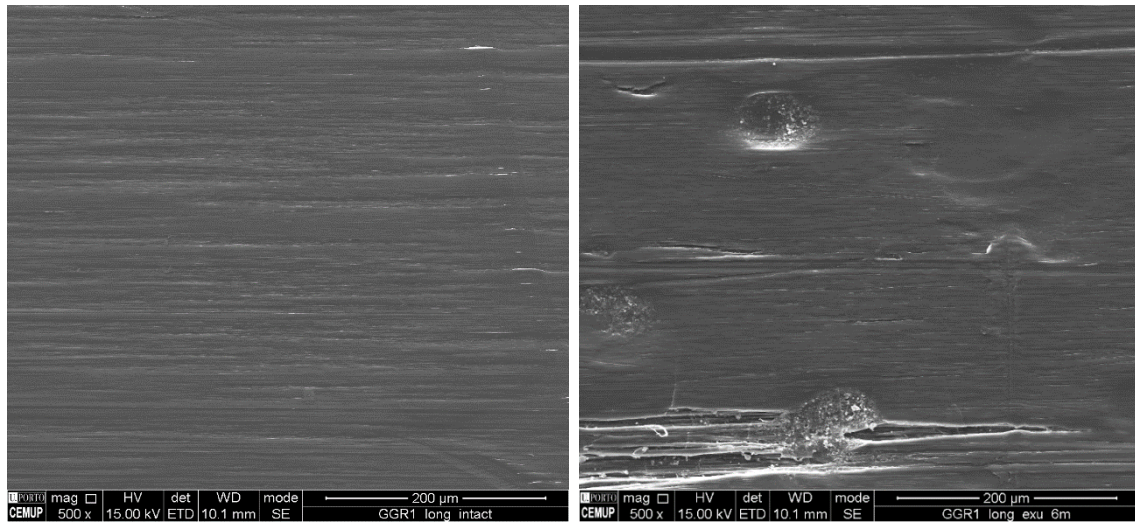
741

742

743

744

745



(a)

(b)

746

747 Figure 6 – SEM images of the longitudinal bars of the geogrid (×500): a) intact
748 specimen; b) exhumed specimen after 6 months.

749

750

751

752

753

754

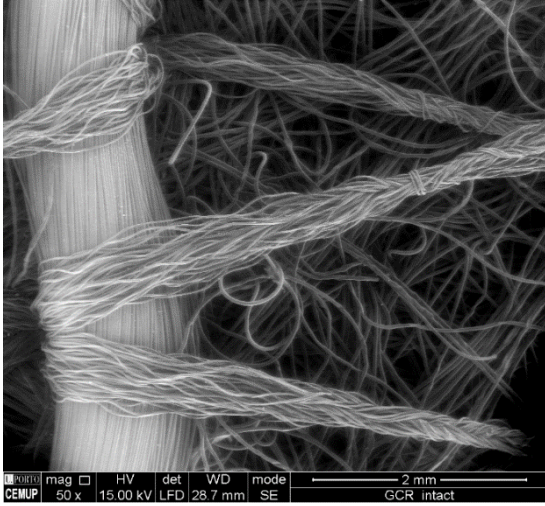
755

756

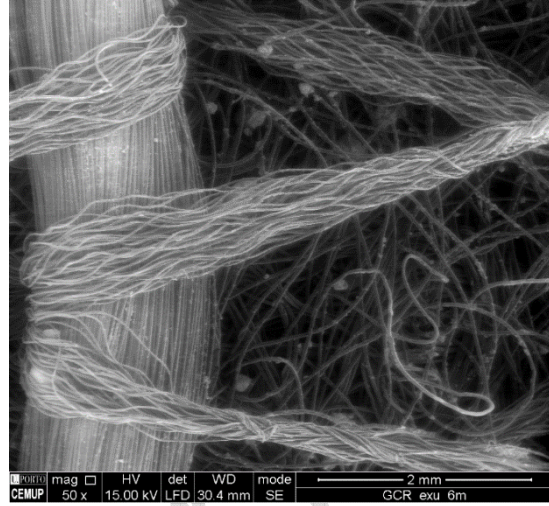
757

758

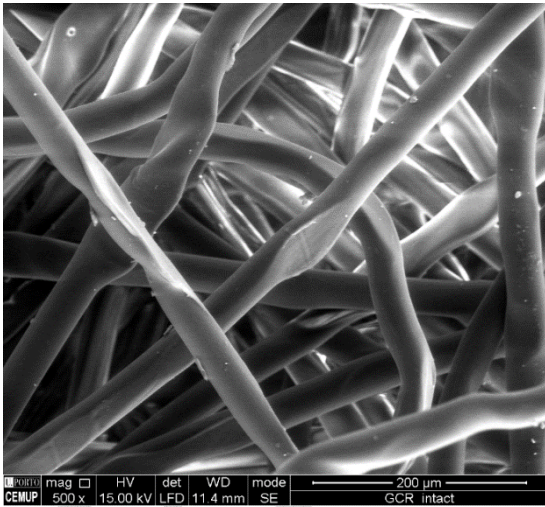
759



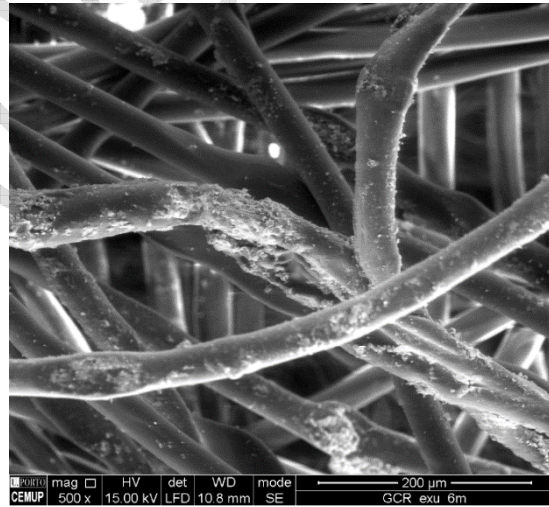
(a)



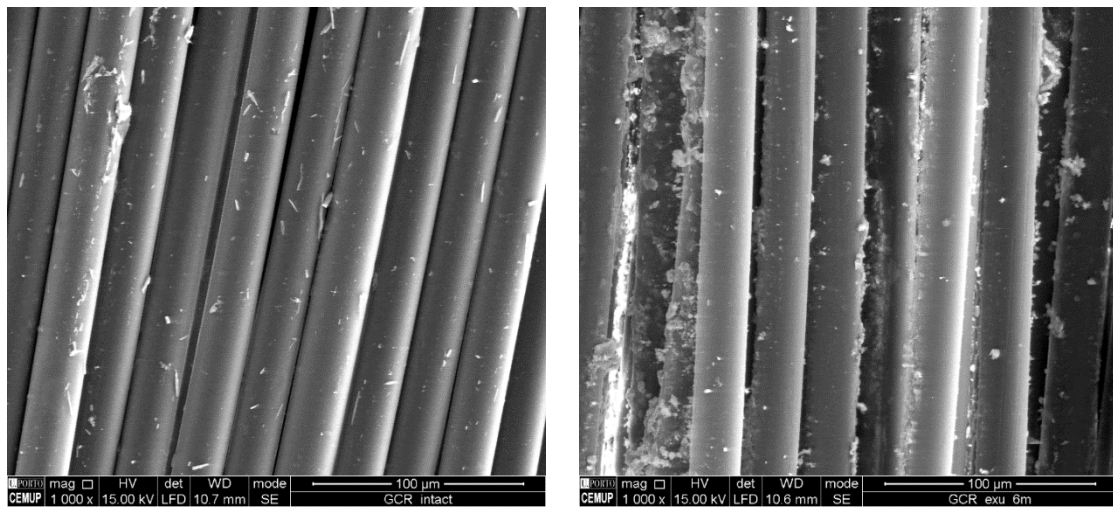
(b)



(c)



(d)



(e)

(f)

760 Figure 7 – SEM images of geocomposite specimens: a) intact ($\times 50$); b) exhumed
761 specimen ($\times 50$); c) intact ($\times 500$); d) exhumed specimen ($\times 500$); e) intact ($\times 1000$);
762 f) exhumed specimen ($\times 1000$).

763

764

765

766

767

768

769

770

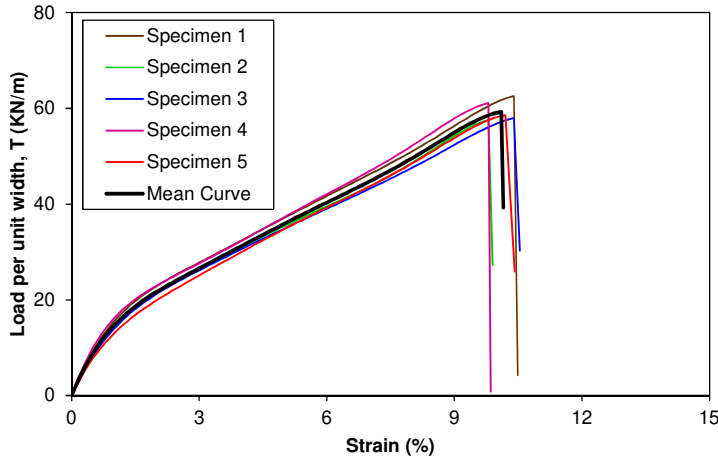
771

772

773

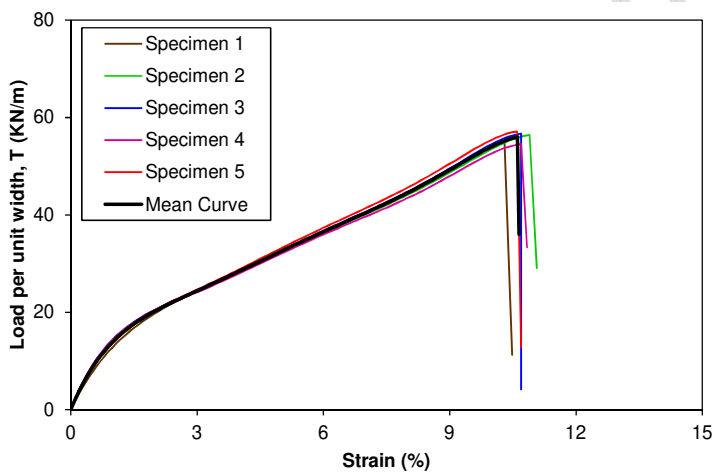
774

775



776

777 (a)



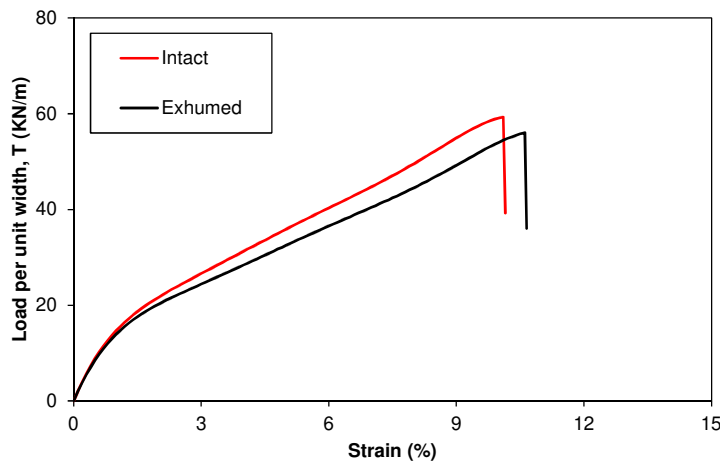
778

779 (b)

780 Figure 8 – Load-strain curves of tensile tests performed on: a) intact geogrid specimens;

781 b) exhumed geogrid specimens.

782



783

784 Figure 9 – Comparison of load-strain curves of intact and exhumed geogrid specimens.

785

786

787

788

789

790

791

792

793

794

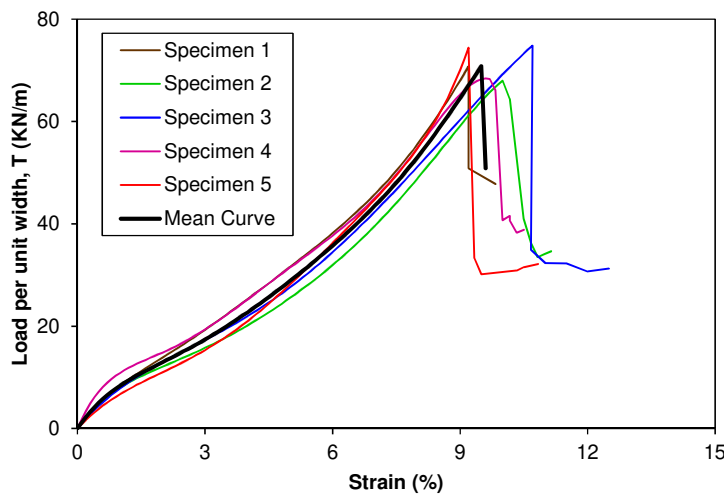
795

796

797

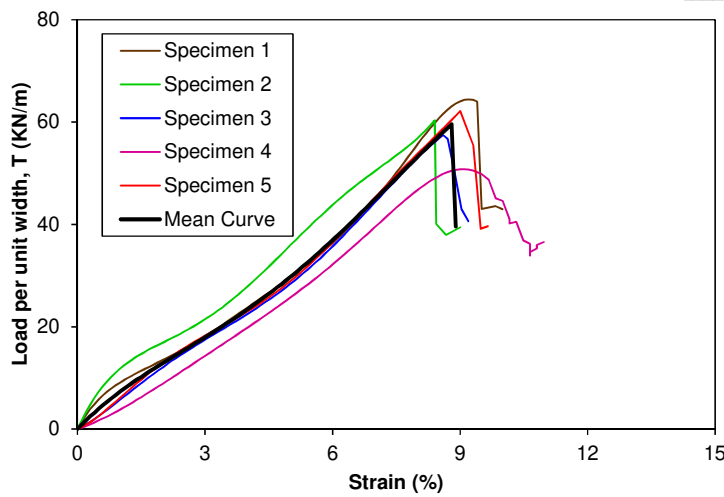
798

799



800

801 (a)



802

803 (b)

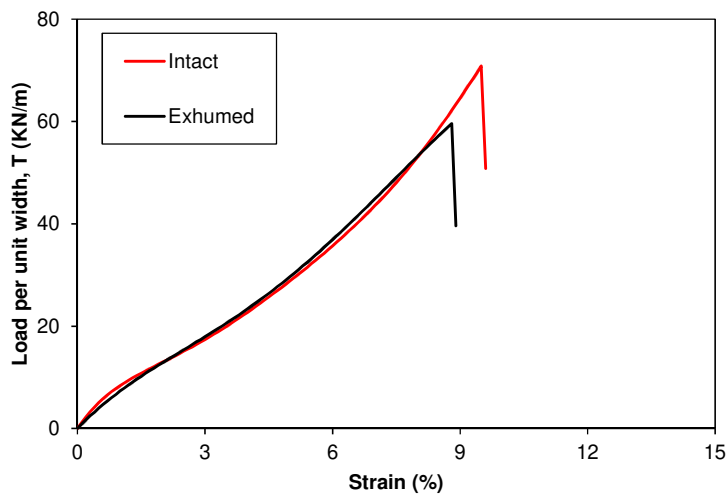
804 Figure 10 – Load-strain curves of tensile tests performed on: a) intact geocomposite
805 specimens; b) exhumed geocomposite specimens.

806

807

808

809



810

811 Figure 11 – Comparison of load-strain curves of intact and exhumed geocomposite

812 specimens.

813

814

Accepted Version